Localization of unbounded contacts on vibrating elastic plates

Maxime Farin, Chloë Palerm, Claire Prada, and Julien de Rosny

Citation: The Journal of the Acoustical Society of America **148**, 3455 (2020); doi: 10.1121/10.0002778
View online: https://doi.org/10.1121/10.0002778
View Table of Contents: https://asa.scitation.org/toc/jas/148/6
Published by the Acoustical Society of America

JASA ARTICLE

Localization of unbounded contacts on vibrating elastic plates

Maxime Farin, Chloë Palerm, Claire Prada, and Julien de Rosny[a)]
Institut Langevin, ESPCI Paris, Université PSL, Sorbonne Université, Université de Paris, CNRS, 75005 Paris, France

ABSTRACT:
Detection and localization of unbounded contacts in industrial structures are crucial for user safety. However, most structural health monitoring techniques are either invasive, power-consuming, or rely on time-varying baseline comparison. A passive acoustic method is proposed to localize unbounded contacts in plate-like structures, using the acoustic emissions by the contacts when they are excited by ambient noise. The technique consists of computing the correlation matrix of the signals measured by a set of receivers and applying to this matrix a beamforming algorithm accounting for flexural wave dispersion. To validate the technique, an experimental setup is developed in which three idealized unbounded contacts are created on a thin plate excited by a shaker. How the quality of the defect localization depends on the defect type, receiver number, and the characteristics of the noise is investigated. Finally, it is shown that the localization of unbounded contacts is possible using either an acoustic ambient noise source or a more realistic jet engine noise. © *2020 Acoustical Society of America*.
https://doi.org/10.1121/10.0002778
(Received 20 May 2020; revised 28 October 2020; accepted 8 November 2020; published online 7 December 2020)
[Editor: Marcel C. Remillieux] Pages: 3455–3466

I. INTRODUCTION

Rapidly detecting and localizing damages such as cracks, delamination, or debonding on solid structures is crucial in industry for user safety and machine performance. Usual verification of structure integrity is performed by visual inspection such as dye penetrant testing (Boller *et al.*, 2009; Diamanti and Soutis, 2010; Katunin *et al.*, 2015). In complement, changes in elastic properties can be monitored with active acoustic methods that use receivers to send acoustic signals in the inspected structure. Linear approaches compare wave transmission through the structure with a reference measurement on the intact structure to highlight the effect of the damage on the wave propagation (pitch-catch or pulse-echo) (Amerini and Meo, 2011; Ihn and Chang, 2008). Nonlinear elastic wave spectroscopy (NEWS) approaches take advantage of the nonlinear behavior of damaged materials (Van Den Abeele *et al.*, 2000; Van Den Abeele *et al.*, 2001). Indeed, it is observed that eigenmode frequencies of damaged structures shift with increasing vibration level (Cawley and Adams, 1979; Rivière *et al.*, 2010; Salawu, 1997). It is the principle of the commonly used "coin-tap" technique (Cawley and Adams, 1988). Furthermore, when a damaged structure is simultaneously excited with a low frequency f_1 and a high frequency f_2, harmonics (e.g., $2f_1$) and mixing (e.g., $f_1 \pm f_2$) of these frequencies appear. Therefore, the amplitude at these added frequencies is a global index of damage apparition and evolution (Amerini and Meo, 2011; Buck *et al.*, 1978; Van Den Abeele *et al.*, 2001; Yang *et al.*, 2018; Young *et al.*, 2019). Recent active techniques use time reversal (TR) to generate ultrasonic pulses at different positions on the structure and either compare the pulses with a reference pulse measured at an undamaged position (Le Bas *et al.*, 2015) or focus a pulse and its inverse and sum them (Bou Matar *et al.*, 2009; Ulrich *et al.*, 2007), to locally highlight the nonlinear response of the structure and therefore image millimeter-size defects [see Anderson *et al.* (2019) for a review of TR-NEWS studies]. However, these active techniques require power sources and full scans of the inspected object to localize the defect. They are therefore difficult to apply for a continuous monitoring.

Passive approaches take advantage of ambient noise to localize defects using a network of receivers. A few years ago, a noise correlation technique (Chehami *et al.*, 2014) was proposed to localize linear defects on thin plates. The localization is obtained by computing the difference of the correlation matrix between the receivers obtained with a defect and the one obtained in the reference healthy structure. However, a baseline comparison is problematic because elastic properties vary with time, temperature, or stress conditions.

To overcome this limitation, we propose a solution in the case of a defect with unbounded contact embedded in a plate-like structure supporting sufficiently high amplitude vibration noise. Such a defect produces clapping and rubbing surfaces that generate wide frequency band elastic waves (Asamene and Sundaresan, 2012; Hase *et al.*, 2012; Joseph *et al.*, 2019). We show that if the defect is excited by low-frequency (LF) ambient noise, it can be localized using a passive acoustic technique based on the cross-correlation of the emitted acoustic signals recorded on a network of receivers. The signal processing procedure implemented to localize the defect is presented in Sec. II. In Sec. III, we

[a)]Electronic mail: julien.derosny@espci.psl.eu

describe an experimental setup to test the localization technique. Different idealized unbounded contact situations are considered on a thin plate excited by a shaker which mimics an ambient noise source. In Sec. IV, the quality of the localization is investigated as a function of the defect type and the excitation amplitude and frequency. The applicability of the technique to detect several unbounded contacts or in an industrial context is discussed in Sec. V.

II. HOW TO LOCALIZE UNBOUNDED CONTACTS FROM ACOUSTIC EMISSIONS

Our aim is to localize an unbounded contact on a plate from its high-frequency (HF) (> 1 kHz) acoustic emissions when it is excited with a lower frequency noise (< 1 kHz). To do so, we have to overcome two major difficulties. First, the wave front emitted by the defect has a long duration and is reflected multiple times off the plate boundaries. Second, the waves propagating in the thin plate are highly dispersive because most of the energy is carried by the bending mode A_0 in the investigated frequency range (1 Hz–50 kHz) (Royer and Dieulesaint, 2000). For example, in the frequency range from 1 to 20 kHz, the group speed increases by a factor of 20. Consequently, the emitted signals significantly spread in time and we cannot distinguish the direct wave front from the reflected ones off the plate boundaries. In reverberating media, if all the Green's functions (responses) between each position on the surface under study and the receiver positions are known, acoustic sources can be localized with only a few receivers by taking advantage of the reverberations (Ing *et al.*, 2005). However, learning the Green's functions requires either a model (analytical or numerical) or an estimation of them during a calibration process, which can be very costly for complex structures. Alternatively, one can detect a source only using the direct path. In such a case, the reflections off the boundaries act as incoherent contributions to the measured signals. Therefore, standard beamforming techniques based on time delay and picking the arrival time of a wave front at several receivers do not apply. We present a method that uses a dense set of receivers to get rid of the reflective part of the recorded signals in order to locate the noise source (unbounded contact). Let $s_i(t)$ be the acoustic signals measured by receivers i ($i = 1, \ldots, N$) when the unbounded contact is excited. It is helpful to write these signals in terms of the Green's functions ($G(\mathbf{r}_d, \mathbf{r}_i, t)$) between the defect position ($\mathbf{r}_d$) and the receiver positions ($\mathbf{r}_i$). Introducing the equivalent source function of the defect $f(t)$,

$$s_i(t) = G(\mathbf{r}_d, \mathbf{r}_i, t) * f(t), \tag{1}$$

where the asterisk is the time convolution product. Note that the source function $f(t)$ is a continuous random signal. In order to tackle the problem of the unknown excitation source function $f(t)$, we cross-correlate the measured signals between receivers, i.e., we compute, in Fourier's domain, the correlation matrix C whose elements are

$$\tilde{C}_{ij}(\omega) = \langle \tilde{s}_i(\omega)_\tau \tilde{s}_j(\omega)_\tau^* \rangle_\tau, \tag{2}$$

where ω is the pulsation and $\tilde{s}_i(\omega)_\tau$ is the Fourier transform of a section of duration τ of the total recorded signal $s_i(t)$. The operator $\langle \cdots \rangle_\tau$ represents the stacking (or averaging) of the products $\tilde{s}_i(\omega)_\tau \tilde{s}_j(\omega)_\tau^*$ over a sliding window for the total duration of the recorded signals. The stack should tend towards

$$\tilde{C}_{ij}(\omega) \approx \tilde{G}(\mathbf{r}_d, \mathbf{r}_j, \omega) \tilde{G}(\mathbf{r}_d, \mathbf{r}_i, \omega)^* \tilde{F}(\omega), \tag{3}$$

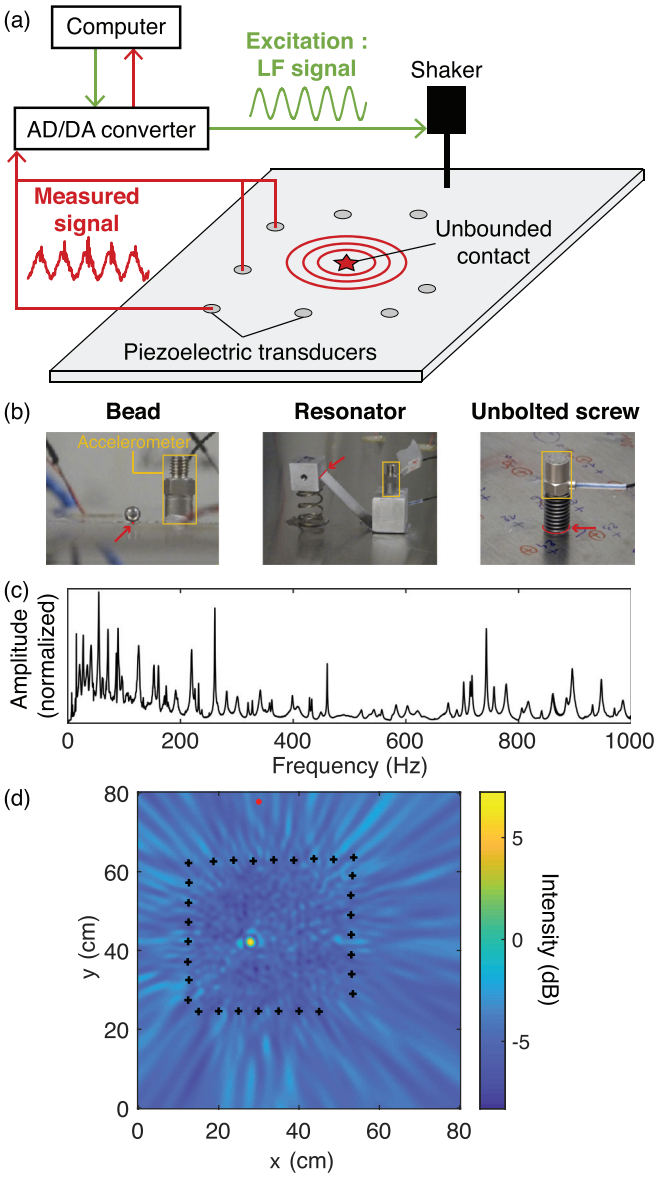

FIG. 1. (Color online) (a) Schematic of the experiment. A thin aluminum plate is attached to a shaker inducing a low-frequency (LF) vibration. A non-linear defect generates a high-frequency (HF) acoustic signal when excited. The acoustic signals are recorded with a network of piezoelectric receivers. (b) The three types of contacts investigated (indicated with a red arrow): a bead (punctual contact), a couple of resonators (frictional contact), and an unbolted screw (threaded interface). An accelerometer measures the plate vibration close to the defect. (c) Amplitude spectrum showing the eigenmodes of the aluminum plate for frequencies below 1 kHz. (d) Localization map of an unbolted screw on the plate (yellow spot). The piezoelectric receivers are indicated by black crosses and the shaker connection with a red dot.

https://doi.org/10.1121/10.0002778

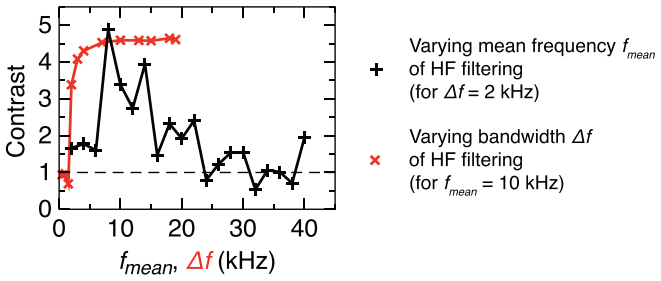

FIG. 2. (Color online) Contrast of the defect spot intensity over the maximum of the secondary lobes intensity for an unbolted screw excited by a random noise of frequency range [200, 300] Hz, when the generated HF signal used for the localization is filtered around different mean frequency f_{mean} with a bandwidth $\Delta f = 2$ kHz or around frequency $f_{mean} = 10$ kHz for different bandwidths Δf.

where $\tilde{F}(\omega)$ is the Fourier transform of the autocorrelation of the random source $f(t)$, thus enhancing the Green's functions $\tilde{G}(\mathbf{r}_d, \mathbf{r}_j, \omega)$ of the wave coming from the defect. Practically, in the following, we record signals of 10 s duration and we stack sections of duration $\tau = 0.3$ s. The sampling frequency is 96 kHz, which leads to a 3.3 Hz frequency resolution of the correlation matrix $\tilde{C}$. To evaluate the defect position, we only need the first arrivals of the wave front coming from the defect in the correlation matrix. Therefore, we select only a time window in $C_{ij}(t)$ of duration 2 ms before and after $t = 0$. It roughly corresponds to the maximum propagation time between the source and the receivers at the lowest considered frequency in the processing (i.e., 1 kHz). This operation significantly decreases the subsequent computation time of the defect localization map. Now that the direct wave contributions are embedded in the correlation matrix, the defect is localized by applying a

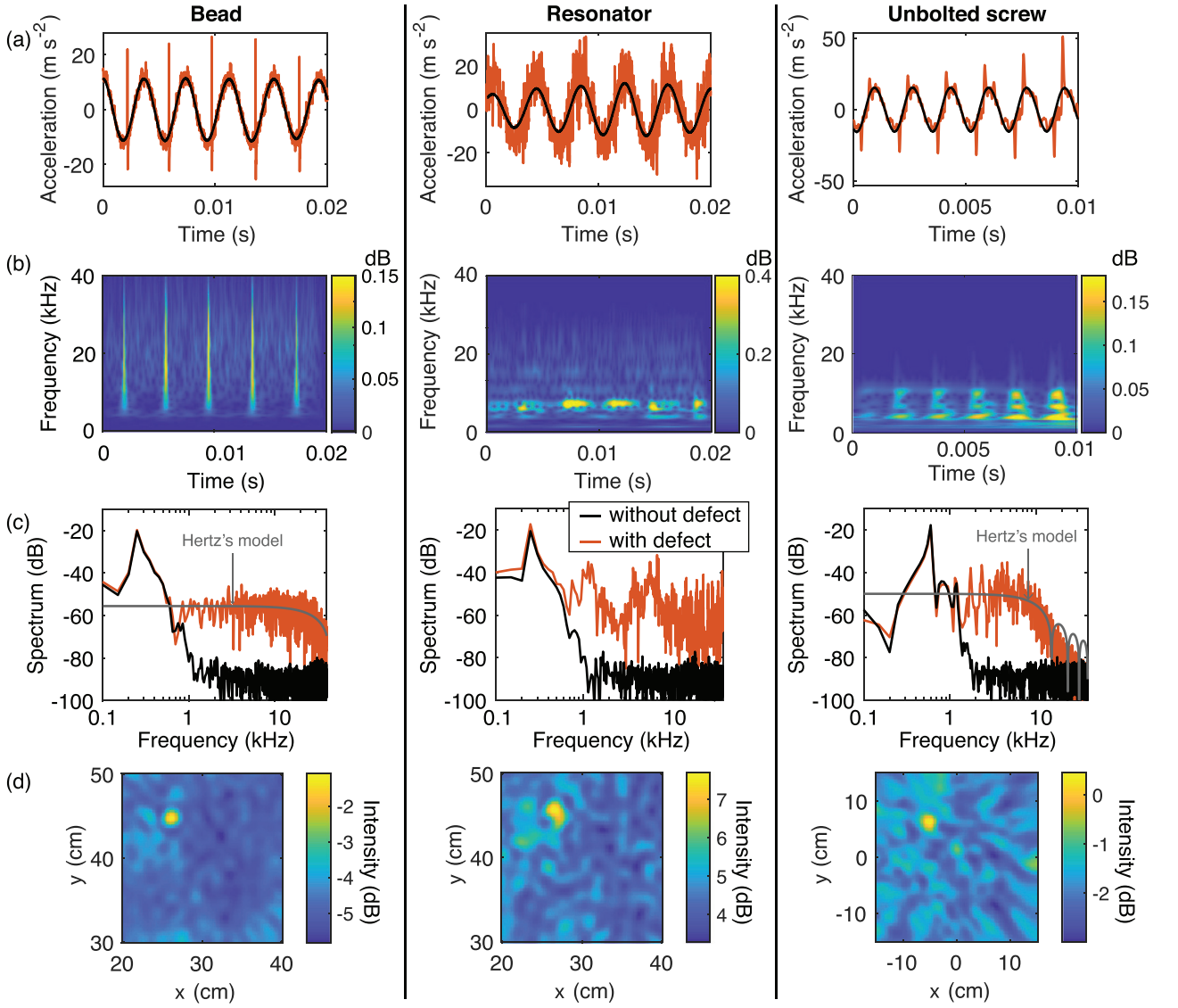

FIG. 3. (Color online) (a) Several periods of the plate vibration measured by an accelerometer when the LF excitation is a continuous sine wave, in the presence (red) and absence (black) of a 4-mm steel bead, a resonator and an unbolted screw. (b) Spectrograms of the red signals. (c) Associated amplitude spectra. The amplitude spectrum of an impact predicted by Hertz's model is shown for the bead and the screw. (d) Map of the localization of the defect, indicated by a yellow spot.

beamforming approach taking dispersion into account. To do so, since the Green's function $\tilde{G}(\mathbf{r}_d, \mathbf{r}_j, \omega)$ appears twice in the correlation matrix, we multiply each side $\tilde{C}_{ij}$ by the weight functions $\phi_i(\mathbf{r}, \omega)$, given by the phase term of the flexural A_0 mode

$$\phi_i(\mathbf{r}, \omega) = e^{-ik(\omega)\|\mathbf{r}-\mathbf{r}_i\|}, \tag{4}$$

where $\|\mathbf{r} - \mathbf{r}_i\|$ is the distance between the receiver i and a point on the plate and $k(\omega)$ is the dispersion relation of A_0 mode. Practically, we compute at position $\mathbf{r}$ the ambiguity function (Heitmeyer *et al.*, 1984), given by

$$\tilde{A}(\mathbf{r}, \omega) = \sum_{i,j} \phi_i(\mathbf{r}, \omega)^* \tilde{C}_{ij}(\omega) \phi_j(\mathbf{r}, \omega). \tag{5}$$

It can be shown that the ambiguity function is maximum when $\mathbf{r} = \mathbf{r}_d$, i.e., at the defect position. We found that a robust approach is to retain only the phase information in the correlation matrix $\tilde{C}_{ij}(\omega)$ by dividing it by its amplitude $|\tilde{C}_{ij}(\omega)|$. The ambiguity is thus insensitive to discrepancies between receiver's sensitivities.

Once the ambiguity function estimated over a frequency band which contains most of the HF energy generated by the defect, excluding the frequency range of the excitation noise, we compute the inverse Fourier transform $a(\mathbf{r}, t)$ of $\tilde{A}(\mathbf{r}, \omega)$. At the defect position ($\mathbf{r} = \mathbf{r}_d$), the direct path contributions coming from the defect interfere constructively in $a(\mathbf{r}, t)$ around time t = 0 over a time interval of duration $1/\Delta f$, where Δf is the bandwidth of the HF signal used for the localization of the unbounded contact. Finally, the integrated ambiguity surface at position $\mathbf{r}$ (i.e., our defect localization map) is given by

$$I(\mathbf{r}) = \int_{-1/2\Delta f}^{1/2\Delta f} |a(\mathbf{r}, t)|^2 \mathrm{d}t. \tag{6}$$

III. EXPERIMENTAL SETUP AND A FIRST EXPERIMENT

Our experimental setup is composed of a 2-mm thick, $80 \times 80\,\mathrm{cm}^2$ thin aluminum plate with an idealized unbounded contact [Fig. 1(a)]. According to Royer and Dieulesaint (2000), the approximate relation of dispersion of the A_0 mode in this plate is $k(\omega) \simeq 0.57\sqrt{\omega}$, using the elastic properties of aluminum. In order to excite the unbounded contact, a shaker (4810, Brüel & Kjaer) is connected to the plate with a piano string and generate a LF (< 1 kHz) excitation vibration. The piano string connection is used to mostly transmit the normal motion of the shaker while diminishing non-linearities. Additionally, both the plate and the shaker are suspended by elastic stretchers to attenuate parasite external vibrations as much as possible. Appendix A shows that the pattern and frequency of measured eigenmodes of the plate compare well with numerical simulations using free boundary conditions. One can therefore assume that our setup exerts only a few constraints on the plate. The LF excitation is of high amplitude (plate vibration acceleration $\sim 0.5 - 5$ g) in order to trigger acoustic emissions by the defect. With this setup, the amplitude at the intended frequency of excitation is about two orders of magnitude higher than the amplitude of its harmonics. We investigate three types of idealized unbounded contacts [Fig. 1(b)].

(1) A bead: a punctual contact created by a steel ball placed on the plate. When the plate vibrates, the bead takes off and impacts the plate multiple times, generating signals of wide frequency bandwidth.
(2) A resonator: a frictional contact is obtained by fixing to the plate a resonator consisting of a cube mounted on a spring which is rubbing against a thin aluminum strip when the plate is excited.
(3) A screw: a threaded interface consisting in a M8 4-cm long unbolted screw impacting and turning on its thread.

Figure 1(c) shows an amplitude spectrum of the aluminum plate vibration below 1 kHz, with spikes corresponding to the frequencies of the plate eigenmodes. When we create an unbounded contact on the plate, we first emit a frequency-modulated signal (chirp) of frequency varying from 100 to 1000 Hz to verify which of these eigenmodes excite the contact. Then, we investigate the response of the unbounded

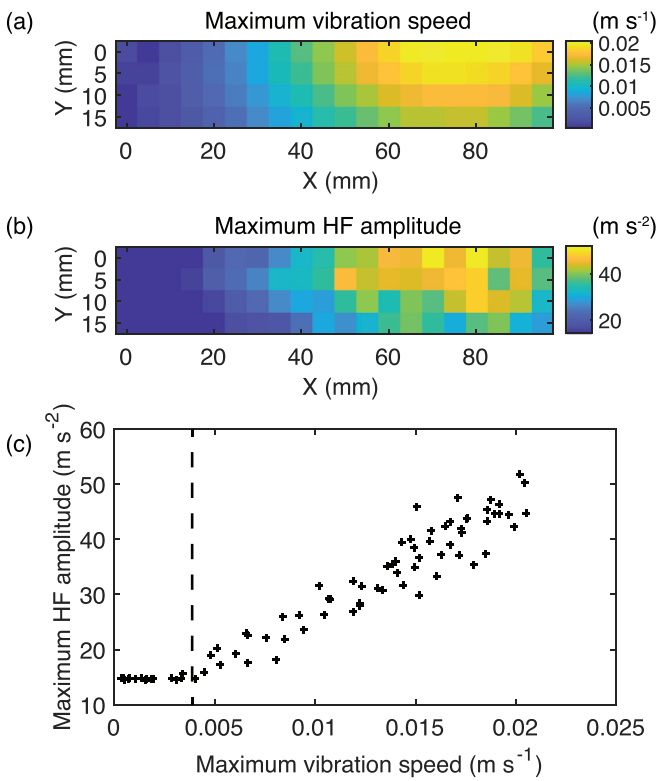

FIG. 4. (Color online) The thin plate is excited with an 860 Hz sine wave. (a) Maximum vibration speed measured with a vibrometer at different positions on the plate. (b) Maximum of the HF acoustic signal (> 1 kHz) generated by a 4-mm bead and measured with an accelerometer, as function of the bead positions. (c) Maximum amplitude of the HF acceleration as a function of the maximum vibration speed for each position of the bead. The threshold vibration speed after which the bead generates HF signal is indicated by a dashed line.

https://doi.org/10.1121/10.0002778

contact to an excitation noise consisting of a random noise filtered around a frequency that excites the contact.

The acoustic emissions by the excited contacts are recorded with a network of 30 piezoelectric receivers (2-cm wide piezoceramic disks). A piezoelectric accelerometer (8309, Brüel & Kjaer) measures the plate vibration close to the defect [Figs. 1(a), 1(b)]. The signals played by the shaker and recorded by the receivers are handled by a 32-channel Analog/Digital audio card (Orion 32, *Antelope*), at a sample rate of 96 to 192 kS/s.

An example of localization of an unbolted screw is shown in Fig. 1(d). To estimate the quality of detection, we introduce the contrast which is the ratio of the intensity at the defect position over the maximum intensity of the secondary lobes. This parameter depends on the frequency range of the HF acoustic signal used for the localization. In Fig. 2, the contrast is plotted with respect to the mean frequency for a fixed bandwidth (and vice versa). We observe that the contrast is maximum around a mean frequency $f_{mean} \simeq 10$ kHz and increases as the bandwidth Δf increases, up to about 10 kHz, after which it stabilizes. The fact that the contrast of the screw localization decreases after $f_{mean} \simeq 10$ kHz is discussed in Sec. IV. In the following, in order to maximize the spot contrast, the measured acoustic signals are always filtered between 1 and 20 kHz and the defect is placed inside the receiver network, unless otherwise specified. In Appendix B, based on a diffuse model, two expressions of the contrast due to the reflections off the boundary and corresponding to two asymptotic regimes are provided. In Appendix C, the effect of the sensor array geometry on the secondary lobes is studied.

IV. ANALYSIS OF THE DEFECT LOCALIZATION

In this section, the localization contrast is investigated for different defects as a function of the excitation noise characteristics.

A. Comparison for three defect types

We now inspect the acoustic response of the investigated defects. The defects are excited with a random noise filtered around an eigenmode (around 260 Hz for the bead and the resonator and around 588 Hz for the screw). All three defects generate very different HF signals [Figs. 3(a)–3(c)].

In the signals generated by the bead and the screw, we observe periodic impulsive signals caused by the successive impacts of the object on the plate [Figs. 3(a), 3(b)]. These impact signals have a wide frequency spectrum [Figs. 3(b), 3(c)]. It is also clearly visible on the amplitude spectra that the 4-mm bead generates higher frequencies at impact than the unbolted screw. Note that the fact that the localization contrast decreases after 10 kHz for the screw in Fig. 2 can be explained by the decreases after 10 kHz of the signal-to-noise ratio of the HF noise generated by the screw [Fig. 3(c)]. The difference of generated frequency range for the bead and the screw can be justified with Hertz's theory of elastic impact between spheres (Hertz, 1882) [also see Johnson (1985)], which shows that the maximum frequency

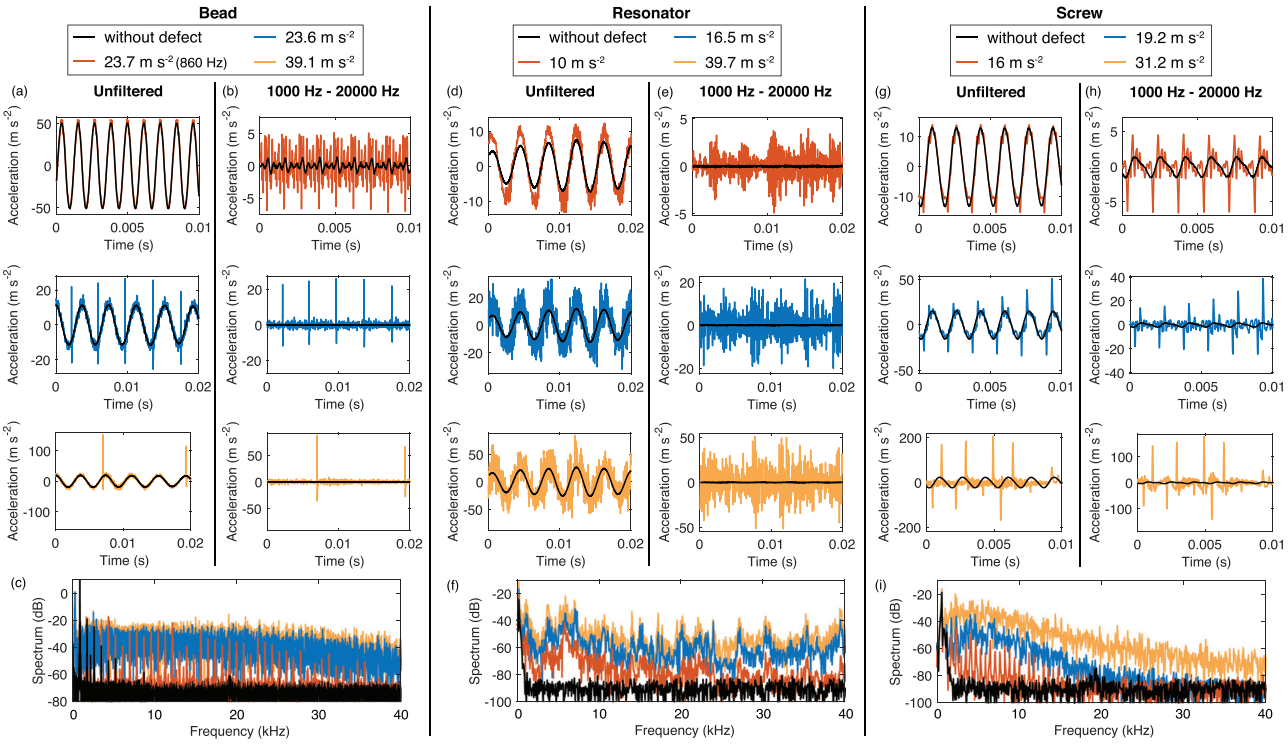

FIG. 5. (Color online) [(a), (d), (g)] Unfiltered and [(b), (e), (h)] filtered signals measured by an accelerometer in the presence (color) and absence (black) of [(a)–(c)] a 4-mm steel bead, [(d)–(f)] a resonator, and [(g)–(i)] an unbolted screw on the plate, for three different amplitudes of an excitation random noise filtered between 200 and 300 Hz (except for one case for the bead where the excitation is an 860 Hz sine wave). [(c), (f), (i)] Amplitude spectra of the acceleration signals shown in (a), (d), and (g).

generated by an impact increases as the size of the impactor decreases. We computed the amplitude spectrum of the force generated by the impact of a single sphere, following Hertz's theory of impact [see Farin *et al*. (2015) for details]. The 4-mm bead generates impacts of duration ∼40 μs, which results in frequencies up to 60 kHz while a sphere of the same mass and elastic properties as the screw but with a contact radius equal to the screw thread generates impacts of duration ∼100 μs, which result in frequencies up to 30 kHz. The frequency range of the computed spectra match well with the measured impact spectra [Fig. 3(c)]. In contrast, the spectrum of the resonator is quite different, with distinguishable spikes in the amplitude spectrum. These spikes correspond to the resonances of the thin aluminum strip on which the resonator is rubbing.

Even though the HF signals generated by the three types of defect are quite different, all defects can be localized with the technique described in Sec. II [Fig. 3(d)]. Note that the bead is the most clearly visible defect. The resonator is an extended source, which results in a slightly wider spot than

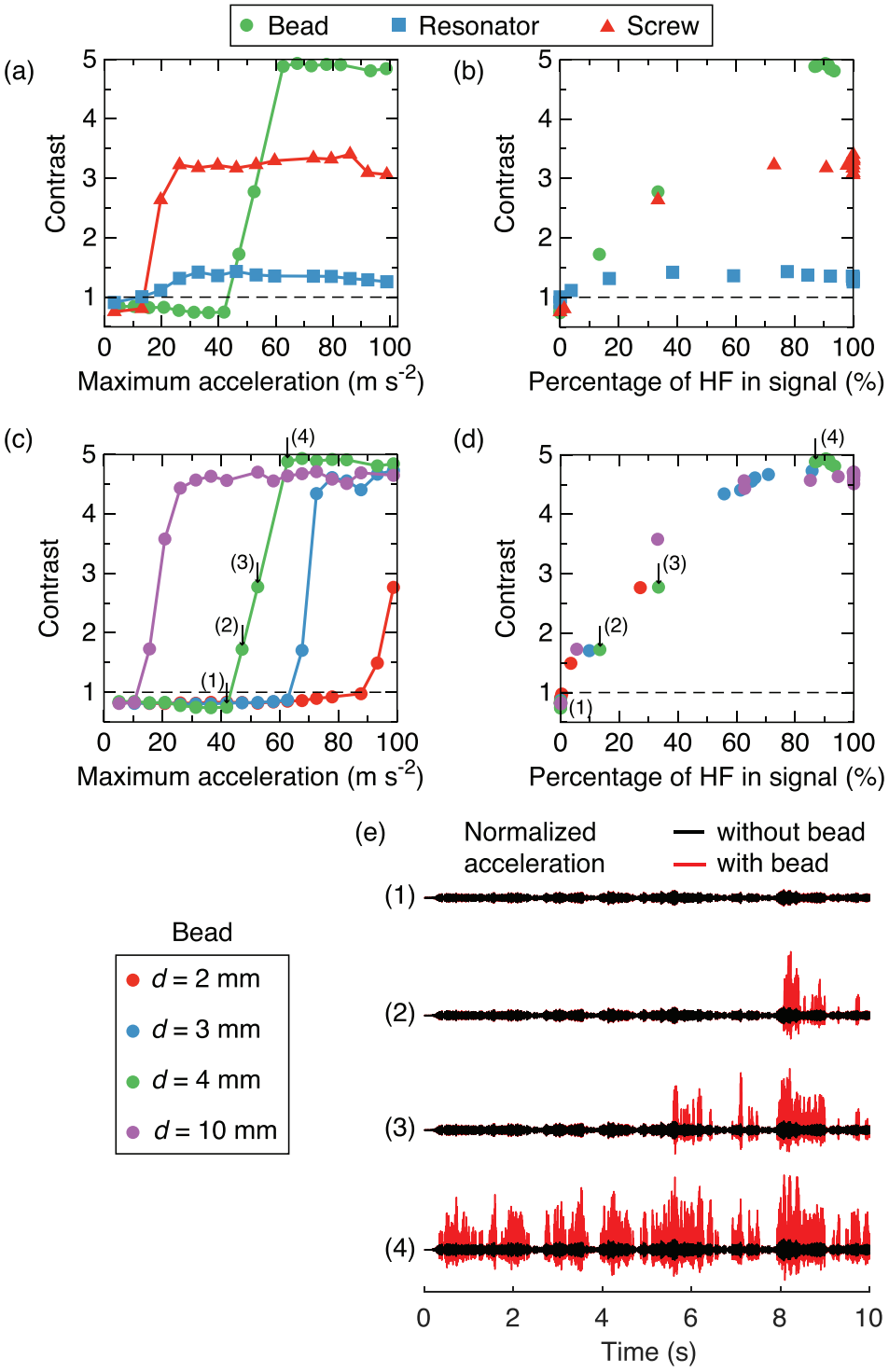

FIG. 6. (Color online) Localization contrast as a function of [(a), (c)] the maximum amplitude measured by an accelerometer on the plate and [(b), (d)] the percentage of HF in the acoustic signal used to localize the defect, for [(a), (b)] the three different types of unbounded contact and [(c), (d)] four different diameters of a bead put on the plate. The plate is excited by a random noise filtered between 200 and 300 Hz. (e) Normalized plate acceleration recorded with (red) and without (black) a 4-mm bead on the plate. In (c) and (d), the data points corresponding to the same maximum acceleration are indicated by numbers.

https://doi.org/10.1121/10.0002778

for the two other defects. The detection contrast depends on the amplitude and frequency of the excitation noise as will be discussed in the following.

B. Influence of plate vibration amplitude

We conduct a simple experiment in order to observe how the acoustic response of an unbounded contact depends on the amplitude of the plate vibration at the defect position. First, a steel bead is moved on a virtual grid by a magnet placed below the plate. For each position of the bead, the plate is excited with an 860 Hz sine wave and the maximum amplitude of the bead HF (> 1 kHz) acoustic response is recorded by an accelerometer. Then, we remove the bead and we record the vibration speed of the plate at each former bead's position using a laser vibrometer (Polytec OFU-505). A good correlation is observed between the vibration amplitude of the plate (i.e., the pattern of the excited eigenmode at frequency 860 Hz) and the amplitude of the HF signal generated by the vibrating bead [Figs. 4(a), 4(b)]. Even though it is trivial that the bead is not excited if it is located on a plate node, it is interesting that the bead remains in contact with the plate for vibration amplitude below a threshold of $\simeq 4$ mm s^{-1} [Fig. 4(c)]. This threshold corresponds to the instant when the plate acceleration is higher than the gravitational acceleration plus the attractive magnet force (divided by bead mass). Above the threshold, the amplitude of the generated HF signal increases linearly with the plate excitation amplitude [Fig. 4(c)].

When we increase the vibration amplitude of the plate, we note an evolving acoustic response of the defects (Fig. 5). When the excitation amplitude is just above the bouncing threshold of the bead and the screw, they jump at every maximum of the LF signal [for the bead, see Figs. 5(a), 5(b) for amplitude 23.7 m s^{-2} and for the screw, see Figs. 5(g), 5(h) for 16 m s^{-2}]. The amplitude spectrum of this periodic HF response is a comb with the excitation frequency and its harmonics [Figs. 5(c), 5(i)]. As the excitation amplitude increases, the bead and the screw jump higher and the period of the HF response becomes twice a period of the LF excitation. Consequently, half the excitation frequency and its harmonics appear in the amplitude spectrum, in addition to the harmonics of the excitation frequencies (not shown). By further increasing the amplitude (or by shifting to a different excitation mode when at the threshold), quarters, eighths and so on of the excitation frequency appear in the spectrum until impacts become unsynchronized with the excitation vibration and the spectrum becomes much richer in frequencies [for the bead, Figs. 5(a), 5(b) for accelerations 23.6 and 39.1 m s^{-2} and for the screw, see Figs. 5(g), 5(h) for accelerations 19.2 and 31.2 m s^{-2}]. For example, this transition towards chaos was described by Tufillaro and Albano (1986). In contrast, such behavior was not observed for the resonator which process of generating HF signals is not caused by impacts but by rubbing of a thin strip against a surface. In this last case, the frequency content of the generated HF noise seems to be the same regardless of the excitation amplitude (after the threshold) and its amplitude seems to increase linearly as the excitation amplitude increases [Figs. 5(d), 5(f)].

We now inspect how the localization contrast is improved when the LF excitation amplitude increases [Fig. 6(a)]. At a given threshold of excitation amplitude, below which the defect remains quiet, the contrast rapidly increases and then saturates. Both the detection threshold and the maximum contrast depend on the type of defect. If we use beads of different diameters, we note that the excitation amplitude threshold decreases as the diameter of the bead increases, but the maximum contrast is unchanged [Fig. 6(c)]. The maximum contrast seems to be controlled by the signal-to-noise ratio (SNR) of the HF signal generated by the defect. The parameter that seems to control the detection threshold (when the contrast exceeds 1), is the percentage of HF in the signal used to locate the defect. This percentage is defined as the percentage of time, over the total signal duration, during which the amplitude of the HF in the signal is higher than the noise level recorded without defects [Figs. 6(b), 6(d), and 6(e)]. The transition between a contrast below 1 and the maximum contrast is controlled by an increasing percentage of HF in the signal. This is particularly clear for the beads of different diameters as all curves collapse when represented as a function of the HF percentage [Fig. 6(d)].

C. Influence of the frequency of the excitation noise

The localization contrast of a defect depends on the frequency range of the excitation noise. The defect can be detected only when the excitation noise includes plate eigenmodes that excites the defect. In theory, increasing the bandwidth of the excitation noise includes more eigenmodes

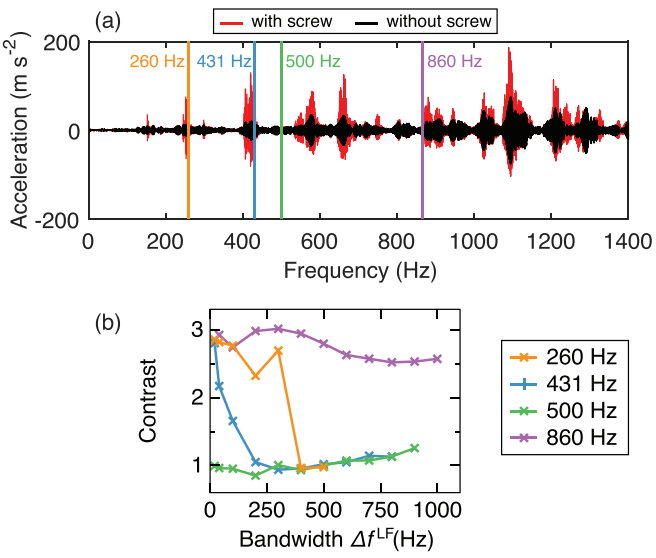

FIG. 7. (Color online) (a) Acceleration signals measured without and with the presence of a screw on the plate when a frequency-modulated signal of frequency varying from 0 to 1400 Hz is emitted. (b) Localization contrast for an unbolted screw excited by a random noise of different central frequencies, as a function of the noise bandwidth Δf^{LF}.

of the plate and the defect should be more efficiently detected. However, this is not trivial in a structure that includes only a few eigenmodes. For example, in Fig. 7(a), only a few modes exciting an unbolted screw below 800 Hz are identified (when the amplitude of the noise generated by the defect is higher than the plate vibration amplitude). In this frequency range, when we emit a random noise centered on an eigenfrequency that excites the defect (e.g., at frequencies 260 or 431 Hz) and we increase the noise bandwidth, there are fewer occasions that the frequency of the noise passes by the exciting eigenfrequency, and the contrast diminishes [Fig. 7(b)]. On the contrary, if the random noise is initially centered around a frequency that does not excite the defect [e.g., 500 Hz in Fig. 7(b)], the defect is not detected if the noise has a narrow bandwidth but it is eventually detected as the bandwidth of the noise increases, as eigenfrequencies exciting the defect become included. In contrast, in a frequency range where the density of eigenfrequencies exciting the defect is high (e.g., above 800 Hz in our plate), increasing the bandwidth of the random noise does not strongly affect the contrast because the probability that the frequency passes by that of an eigenmode that excites the defect remains high [see the curve for 860 Hz in Fig. 7(b)].

V. TOWARDS MORE REALISTIC CONDITIONS

A. Case of several defects

We inspect a case with several defects on the plate. We saw in Sec. IV B that one can only detect defects at the antinodes of the excitation modes. When five unbolted screws are simultaneously placed at different positions on a thin plate, when we play a frequency modulated signal of frequency increasing with time from 450 to 650 Hz, the localization map successively highlights the different screw positions (Fig. 8). Most of the time, one can detect the defect

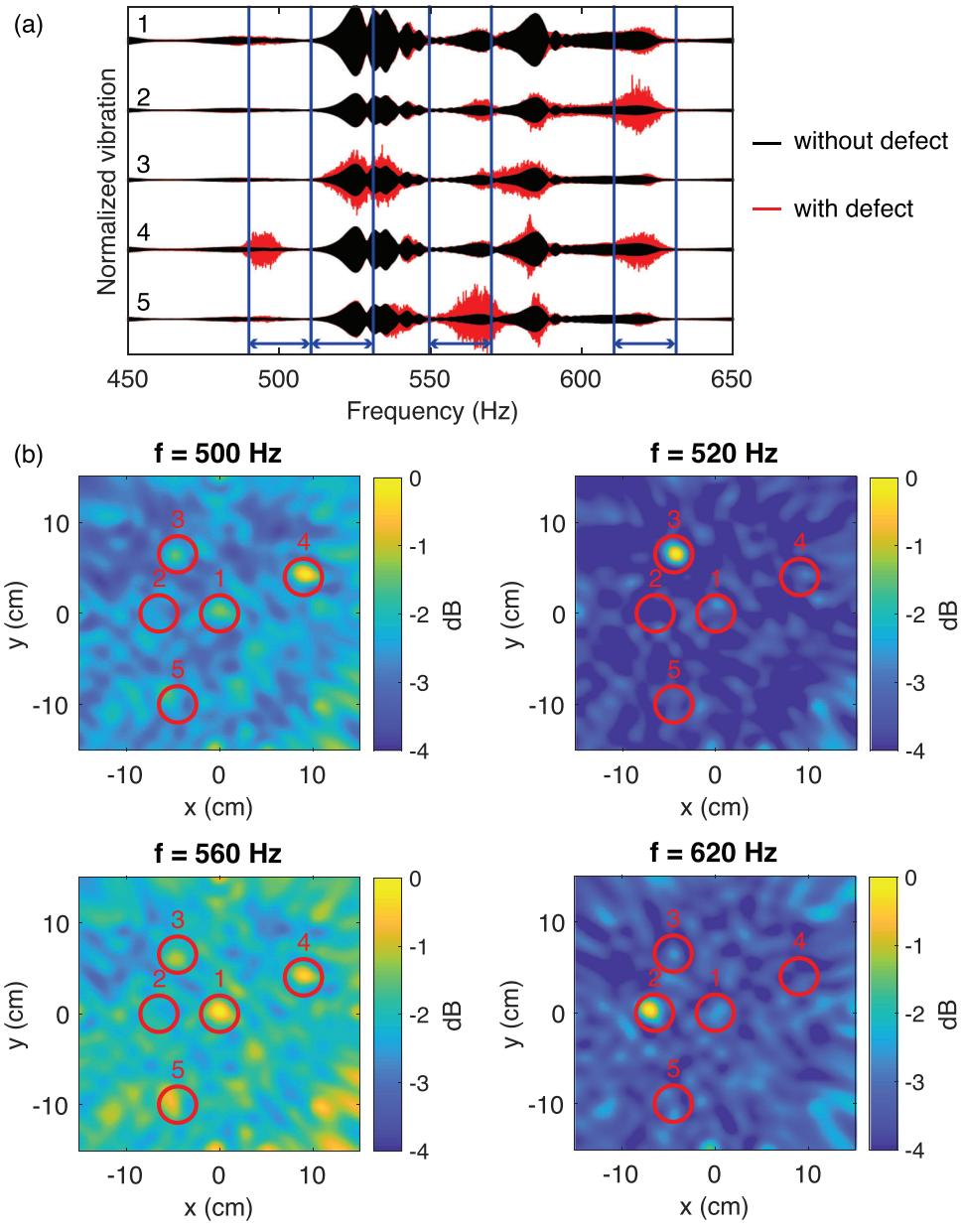

FIG. 8. (Color online) (a) Normalized acceleration signal measured on the plate when the shaker emits a modulated signal of frequency varying from 450 to 650 Hz, with (red) and without (black) the unbolted screw. Each line corresponds to different screw positions. (b) Localization maps obtained using measured signal of bandwidth indicated by the blue line on (a), with five unbolted screws installed simultaneously at the positions indicated by red circles. Position numbers in (b) correspond to the signal numbers in (a).

https://doi.org/10.1121/10.0002778

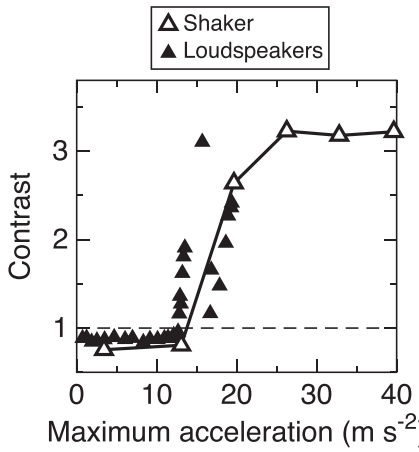

FIG. 9. (a) Contrast of the localization spot as a function of the plate maximum acceleration for an unbolted screw excited by a random noise of frequency range $[200, 300]$ Hz played by the shaker (empty triangles) and by four loudspeakers placed in front of the plate (full triangles).

that generate the highest acoustic amplitude at a given excitation mode [for example, modes $f = 500$, 520, and 620 Hz, Fig. 8(b)]. For some modes, one can detect several defects, although with a less good contrast than when only one defect is detected (for example, mode $f = 560$ Hz). Therefore, the best way to detect the different defects is to successively excite different eigenmodes of the plate. However, practically the ambient noise has a large bandwidth and the detected defects will be the ones that generate the highest amplitude HF acoustic signals.

B. Realistic ambient noise

We have seen that one can detect an unbounded contact using random low frequency vibration. However, these proofs of concept are still far from an aeronautic application. We now inspect more realistic sources of ambient noise. First, we replace the shaker by four loudspeakers installed in front of the plate. We use an unbolted screw as the unbounded contact for this experiment because it is excited at lower excitation amplitudes than the two other defects [Fig. 6(a)]. The loudspeakers emit a random noise filtered between 200 and 300 Hz to excite the screw. It results that we can also localize the defect with this contactless noise source (Fig. 9). Besides, the localization contrast is similar to when we use a shaker emitting the same noise. However, these loudspeakers are not powerful enough to generate as high a plate vibration amplitude as the shaker. The unbolted screw was localized when the acoustic power emitted by the loudspeakers was higher than 94.3 dB, which is much less than the acoustic power emitted by a jet engine (∼120 dB), for example.

In a second experiment, in order to mimic a more realistic ambient noise than a random generated noise, we emitted with the shaker the noise recorded by a microphone in front of a jet engine. The amplitude spectrum of the engine noise shows than vibration energy is mostly in a frequency range below 5 kHz, with frequencies up to 10 kHz [Fig. 10(a)]. When this excitation noise is played in our setup, an unbolted screw generates an acoustic signal with frequencies up to 20 kHz, and can therefore be localized [Fig. 10(b)]. For a given vibration amplitude of the plate, the screw localization contrast is even higher with the engine noise than with a random noise in the same frequency range (100 Hz to 10 kHz).

Therefore, these two experiments show that the presented localization technique can be used with more realistic excitation sources and noises than the ones (shaker and random noise) we used in the previous validating experiments. Other unbounded contact situations (delamination, cracks) need, however, to be investigated in future research.

VI. CONCLUSIONS

A passive acoustic technique has been presented to localize unbounded contacts on a plate-like structure from the acoustic emissions of the defects excited by ambient

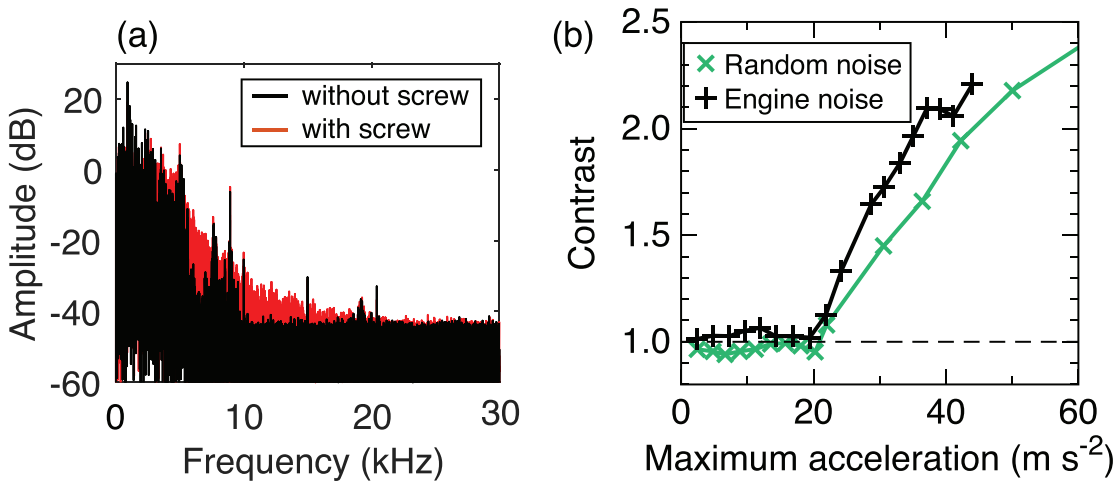

FIG. 10. (Color online) (a) Amplitude spectrum of the signal recorded by an accelerometer when an engine noise is played by the shaker with and without an unbolted screw on the plate. (b) Contrast of the localization spot as a function of the plate maximum acceleration for an unbolted screw excited by a random noise of frequency range $[0.1, 10]$ kHz (green $\times$) and by the engine noise (black $+$).

noise. In order to test the technique, we have investigated three idealized unbounded contact situations on a thin plate excited by a shaker emitting a random noise. We studied how the contrast of the defect localization depends on the type of contact, the amplitude and frequency range of the excitation noise, and the receiver network arrangement. We showed that such defects can be successfully localized when the shaker is replaced by a contactless excitation source and when the excitation noise is a realistic jet engine noise. More work is required to test the presented technique with realist defects encountered in the industry such as cracks or delamination. In our setup, we focused on the bending A_0 modes in thin plates to localize the defects, but symmetrical S_0 Lamb modes may be more sensitive to such types of defects (Ihn and Chang, 2003). Although industrial structures often have a complex shape and are composed of composite materials, which are more heterogeneous than an aluminum plate, we expect the presented technique to be more efficient because these structures have a high eigenmodes density. The condition for defect detection is that the excitation noise amplitude is sufficiently high so that the amplitude of the bending wave generated by the defect can be detected.

ACKNOWLEDGMENTS

This work was supported by Grant No. ANR-17-CE08-0013 (PANSCAN).

APPENDIX A: SOME EIGENMODES OF THE PLATE

In this appendix, we compare five eigenmodes of the investigated aluminum plate measured with a laser vibrometer with that simulated with COMSOL MULTIPHYSICS (see Fig. 11). In the simulations, we set free boundary conditions. The measured and simulated frequencies and patterns of the eigenmodes compare well. Therefore, one can assume that our setup exerts few constrains on the plate.

APPENDIX B: QUALITATIVE DISCUSSION ON THE LOCALIZATION CONTRAST

In this appendix, we evaluate how the contrast of the defect localization depends on the characteristic attenuation time in the plate and on the eigenmode density. Let G_A and G_B be the Green's functions (GF) between the source and sensors A and B, respectively. The GF can be decomposed into two contributions,

$$G_i = G_i^0 + \delta G_i, \tag{B1}$$

where G_i^0 is the direct wave front (free space) and δG_i^0 is the reflected wave field. At the source position and at time $t = 0$, the ambiguity function is

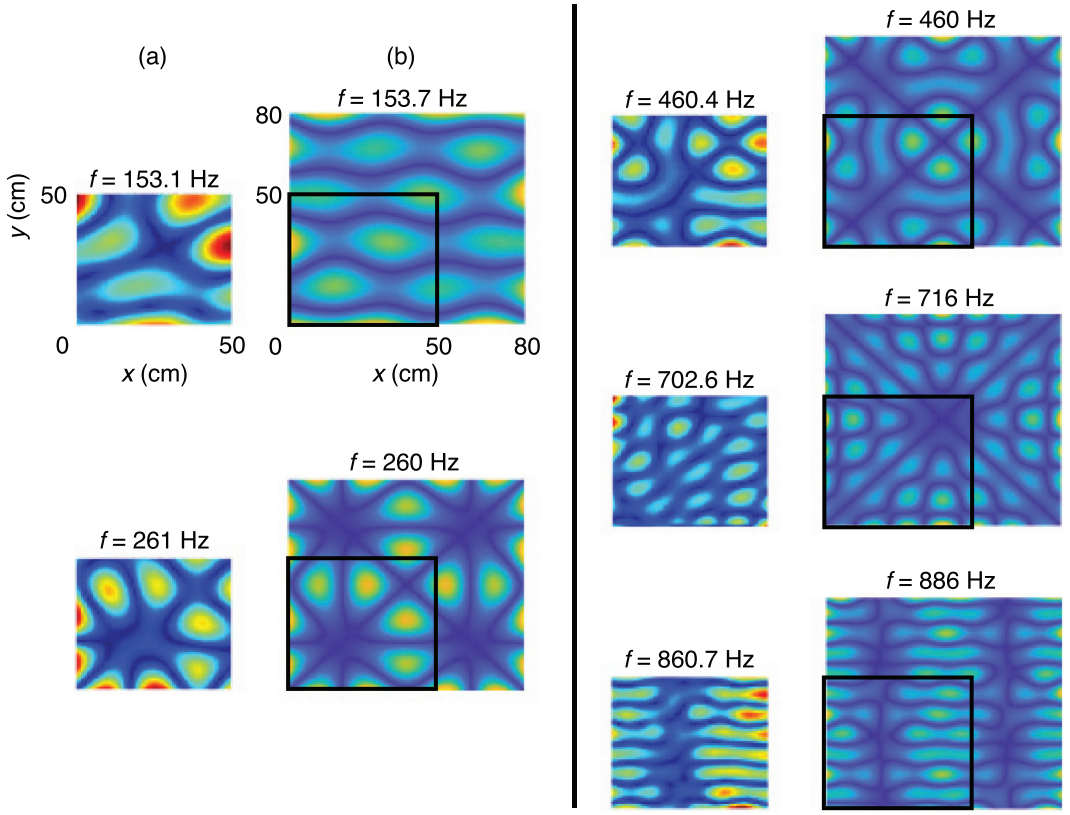

FIG. 11. (Color online) Comparison of the pattern and frequency of five eigenmodes of the aluminum plate, (a) partially measured using a laser vibrometer and (b) simulated with COMSOL MULTIPHYSICS using free boundary conditions.

https://doi.org/10.1121/10.0002778

$$a(0) = \int G_A^{0*}(G_A^0 + \delta G_A)(G_B^0 + \delta G_B)^* G_B^0 \mathrm{d}\omega, \tag{B2}$$

$$= \underbrace{\int G_A^{0*} G_A^0 G_B^0 G_B^{0*} \mathrm{d}\omega}_{a_1} + \underbrace{\int G_A^{0*} G_A^0 \delta G_B^* G_B^0 \mathrm{d}\omega}_{a_2}$$

$$+ \underbrace{\int G_A^{0*} \delta G_A G_B^{0*} G_B^0 \mathrm{d}\omega}_{a_3}, \tag{B3}$$

$$+ \underbrace{\int G_A^{0*} \delta G_A \delta G_B^* G_B^0 \mathrm{d}\omega}_{a_4}. \tag{B4}$$

The frequency dependence of the Green's function is not written for simplicity. The amplitude on the localization map at the source position is related to the term a_1. Its amplitude is given by

$$a_1 = \int G_A^{0*} G_A^0 G_B^0 G_B^{0*} \mathrm{d}\omega \approx \Delta\omega |G_A^0|^2 |G_B^0|^2, \tag{B5}$$

with $\Delta\omega$ is the bandwidth of the recorded signal and $|G_A^0|$ and $|G_B^0|$, the modulus of the free space GF. The contrast is defined as the ratio of the energy of this contribution to the ones due to the reflections. These contributions that degrade the source localization are given by $\langle |a_2|^2 \rangle$ and $\langle |a_3|^2 \rangle$, where $\langle \cdots \rangle$ stands for the averaging over the diffuse field statistics. Indeed, the mean values of a_2, a_3, a_4 are equal to zero and because we assume that the reflection amplitude is weaker than the direct path, $\langle |a_4|^2 \rangle$ is negligeable. As a consequence, the contrast is given by

$$C = \frac{a_1^2}{\langle |a_2|^2 \rangle + \langle |a_3|^2 \rangle}. \tag{B6}$$

The value $\langle |a_2|^2 \rangle$ is worked out from

$$\langle |a_2|^2 \rangle = \int\int G_A^0(\omega) G_A^{0*}(\omega) G_B^0(\omega) G_A^{0*}(\omega') G_A^0(\omega') \times G_B^{0*}(\omega') \langle \delta G_B(\omega') \delta G_B^*(\omega) \rangle \mathrm{d}\omega \mathrm{d}\omega', \tag{B7}$$

$$\approx \Delta\omega \delta\omega |G_A^0|^4 |G_B^0|^2 \langle |\delta G_B|^2 \rangle, \tag{B8}$$

where $\delta\omega$ is the frequency correlation length of the reverberated field. Note that because we assume that the distance between the source and the positions A and B are of the same order, $|G_A| \approx |G_B|$. Let us introduce R as the typical distance between the source and positions A (and B). Due to energy conservation,

$$|G_A|^2 = \frac{P_0 Z}{\pi R}, \tag{B9}$$

where P_0 the power radiated by the source and Z the intrinsic impedance. We now determine the amplitude of $|\delta G_B|^2$. The mean diffuse energy density in a cavity is given by

$$\epsilon = \frac{\langle |\delta G_B|^2 \rangle}{Zc}, \tag{B10}$$

where c is the wave speed. The total energy E for a plate of surface S is simply given by

$$E \approx \frac{|\delta G_B|^2 S}{Zc}. \tag{B11}$$

The link between the power of the source and the energy is

$$P_0 = -\frac{dE}{dt} = \frac{E}{\tau}, \tag{B12}$$

where τ is the characteristic decay time of the cavity. Finally,

$$|\delta G_B|^2 \approx \frac{\tau Z c}{S} P_0. \tag{B13}$$

Because $\langle |a_2|^2 \rangle = \langle |a_3|^2 \rangle$, the contrast is

$$C \approx \frac{1}{2} \frac{\Delta\omega}{\delta\omega} \frac{S}{\pi R \tau c}. \tag{B14}$$

In the case where the attenuation is strong, i.e., when $\tau \ll n$ (n is the modal density), the modes are not "resolved," and the frequency correlation length $\delta\omega$ is given by $1/\tau$, therefore

$$C \approx \frac{1}{2} \frac{S\Delta\omega}{\pi R c}. \tag{B15}$$

It does not depend on the characteristic decay time τ. On the contrary, when the attenuation is low ($\tau \gg n$), $\delta\omega \approx 1/n$, and the contrast is

$$C \approx \frac{1}{2} \frac{S\Delta\omega n}{\pi R \tau c}. \tag{B16}$$

In this case, the larger the decay time and the worst the contrast. In the case of an array of N receivers, it is straightforward to show that the previous expression becomes

$$C \approx \frac{1}{2} \frac{NS\Delta\omega n}{\pi R \tau c}. \tag{B17}$$

Note that this derivation does not take into account secondary lobes due to the sensor array geometry.

APPENDIX C: RECEIVER NETWORK

In this appendix, we investigate the influence of the receiver network arrangement on the localization contrast. When the receivers are arranged uniformly around the defect, we observe that the defect is detected using only four receivers [Fig. 12(a)]. Then, the contrast linearly increases as the number of receivers increases and reaches a maximum for 20 receivers. Using more receivers does not improve the contrast in our configuration. In our experiments, the defect was placed inside the receiver network to have an optimal opening of the network. Practically, more realistic receiver network geometries are along a line or a

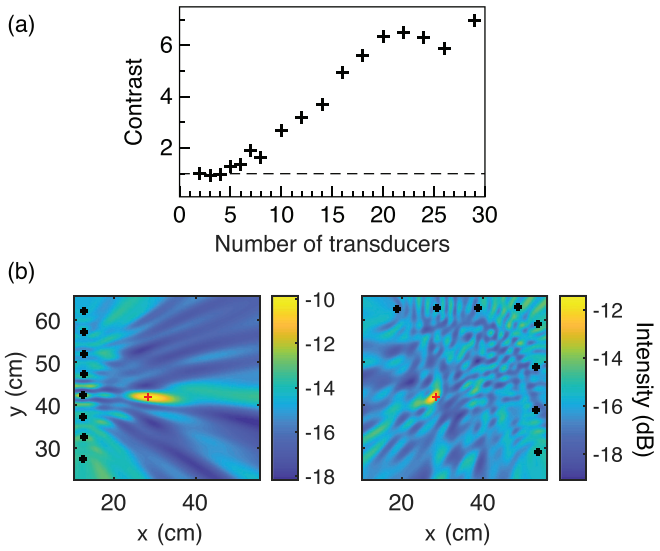

FIG. 12. (Color online) (a) Localization contrast of the localization spot for a 10-mm bead as a function of the number of receivers arranged uniformly around the defect. (b) Localization maps obtained using a line or corner arrangement of an eight-receiver network.

corner. We also tested these two simpler geometries using only eight receivers and we still efficiently detect the defect [Fig. 12(b)].

Amerini, F., and Meo, M. (**2011**). "Structural health monitoring of bolted joints using linear and nonlinear acoustic/ultrasound methods," Struct. Health Monit. **10**(6), 659–672.

Anderson, B., Remillieux, M., Le Bas, P.-Y., and Ulrich, T. (**2019**). *Time Reversal Techniques. Nonlinear Ultrasonic and Vibro-Acoustical Techniques for Nondestructive Evaluation* (Springer, Berlin), pp. 547–581.

Asamene, K., and Sundaresan, M. (**2012**). "Analysis of experimentally generated friction related acoustic emission signals," Wear **296**, 607–618.

Boller, C., Chang, F., and Fujino, Y. (**2009**). *Encyclopedia of Structural Health Monitoring* (Wiley, New York).

Bou Matar, O., Li, Y., and Van Den Abeele, K. (**2009**). "On the use of a chaotic cavity transducer in nonlinear elastic imaging," Appl. Phys. Lett. **95**, 141913.

Buck, O., Morris, W., and Richardson, J. (**1978**). "Acoustic harmonic generation at unbonded interfaces and fatigue cracks," Appl. Phys. Lett. **33**, 371–373.

Cawley, P., and Adams, R. (**1979**). "The location of defects in structures from measurements of natural frequencies," J. Strain Anal. **14**(2), 49–57.

Cawley, P., and Adams, R. (**1988**). "The mechanics of the coin-tap method of non-destructive testing," J. Sound Vib. **122**, 299–316.

Chehami, L., Moulin, E., de Rosny, J., Prada, C., Bou Matar, O., Benmeddour, F., and Assaad, J. (**2014**). "Detection and localization of a defect in a reverberant plate using acoustic field correlation," J. Appl. Phys. **115**, 104901.

Diamanti, K., and Soutis, C. (**2010**). "Structural health monitoring techniques for aircraft composite structures," Prog. Aerosp. Sci. **46**, 342–352.

Farin, M., Mangeney, A., Toussaint, R., de Rosny, J., Shapiro, N., Dewez, T., Hibert, C., Mathon, C., Sedan, O., and Berger, F. (**2015**). "Characterization of rockfalls from seismic signal: Insights from laboratory experiments," J. Geophys. Res. Solid Earth **120**, 7102–7137, https://doi.org/10.1002/2015JB012331.

Hase, A., Mishina, H., and Wada, M. (**2012**). "Correlation between features of acoustic emission signals and mechanical wear mechanisms," Wear **292-293**, 144–150.

Heitmeyer, R., Fizell, R., and Moseley, W. (**1984**). "Full field ambiguity function processing in a complex shallow-water environment," technical report.

Hertz, H. (**1882**). "Über die Berührung fester elastischer Körper" ("On the vibration of solid elastic bodies"), J. Reine Angew. Math. **92**, 156–171.

Ihn, J.-B., and Chang, F.-K. (**2003**). "Detection and monitoring of hidden fatigue crack growth using a built-in piezoelectric sensor/actuator network: I. Diagnostics," Smart Mater. Struct. **13**, 609–620.

Ihn, J.-B., and Chang, F.-K. (**2008**). "Pitch-catch active sensing methods in structural health monitoring for aircraft structures," Struct. Health Monit. **7**(1), 5–19.

Ing, R. K., Quieffin, N., Catheline, S., and Fink, M. (**2005**). "In solid localization of finger impacts using acoustic time-reversal process," Appl. Phys. Lett. **87**(20), 204104.

Johnson, K. (**1985**). *Contact Mechanics* (Cambridge University Press, Cambridge).

Joseph, R., Bhuiyan, M., and Giurgiutiu, V. (**2019**). "Acoustic emission from vibration of cracked sheet-metal samples," Eng. Fract. Mech. **217**, 106544.

Katunin, A., Dragan, K., and Dziendzikowski, M. (**2015**). "Damage identification in aircraft composite structures: A case study using various non-destructive testing techniques," Comp. Struct. **127**, 1–9.

Le Bas, P.-Y., Remillieux, M., Pieczonka, L., Ten Cate, J., Anderson, B., and Ulrich, T. (**2015**). "Damage imaging in a laminated composite plate using an air-coupled time reversal mirror," Appl. Phys. Lett. **107**, 184102.

Rivière, J., Renaud, G., Haupert, S., Talmant, M., Laugier, P., and Johnson, P. (**2010**). "Nonlinear acoustic resonances to probe a threaded interface," J. Appl. Phys. **107**, 124901.

Royer, D., and Dieulesaint, E. (**2000**). *Elastic Waves in Solids I: Free and Guided Propagation* (Springer, Berlin).

Salawu, O. (**1997**). "Detection of structural damage through changes in frequency: A review," Eng. Struct. **19**, 718–723.

Tufillaro, N., and Albano, A. (**1986**). "Chaotic dynamics of a bouncing ball," Am. J. Phys. **54**, 939–944.

Ulrich, T., Sutin, A., Guyer, R., and Johnson, P. (**2007**). "Time reversal and non-linear elastic wave spectroscopy (TR NEWS) techniques," Int. J. Non-Linear Mech. **43**(3), 209–216.

Van Den Abeele, K. E.-A., Johnson, P., and Sutin, A. (**2000**). "Nonlinear elastic wave spectroscopy (NEWS) techniques to discern material damage, Part I: Nonlinear wave modulation spectroscopy (NWMS)," Res. Nondest. Eval. **12**, 17–30.

Van Den Abeele, K. E.-A., Sutin, A., Carmeliet, J., and Johnson, P. (**2001**). "Micro-damage diagnostics using nonlinear elastic wave spectroscopy (NEWS)," NDT&E Int. **34**, 239–248.

Yang, Y., Ng, C.-T., Kotousov, A., Sohn, H., and Lim, H. (**2018**). "Second harmonic generation at fatigue cracks by low-frequency Lamb waves: Experimental and numerical studies," Mech. Syst. Sign. Process. **99**, 760–773.

Young, S., Anderson, B., Hogg, S., Le Bas, P.-Y., and Remillieux, M. (**2019**). "Nonlinearity from stress corrosion cracking as a function of chloride exposure time using the time reversed elastic nonlinearity diagnostic," J. Acoust. Soc. Am. **145**, 382–391.